Dimensional crossover in layered f-electron superlattices

Yasuhiro Tada,[1,*] Robert Peters,[2] and Masaki Oshikawa[1]
[1]*Institute for Solid State Physics, The University of Tokyo, Kashiwa 277-8581, Japan*
[2]*Department of Physics, Kyoto University, Kyoto 606-8502, Japan*
(Received 25 March 2013; revised manuscript received 13 September 2013; published 18 December 2013)

Motivated by the remarkable experimental realizations of f-electron superlattices, e.g., $CeIn_3/LaIn_3$ and $CeCoIn_5/YbCoIn_5$ superlattices, we analyze the formation of heavy electrons in layered f-electron superlattices by means of the dynamical mean field theory. We show that the spectral function exhibits formation of heavy electrons in the entire system below a temperature scale T_0. However, in terms of transport, two different coherence temperatures T_x and T_z are identified in the in-plane and the out-of-plane resistivity, respectively. Remarkably, we find $T_z < T_x \sim T_0$ due to scatterings between different reduced Brillouin zones. The existence of these two distinct energy scales implies a crossover in the dimensionality of the heavy electrons between two and three dimensions as temperature or layer geometry is tuned. This dimensional crossover would be responsible for the characteristic behaviors in the magnetic and superconducting properties observed in the experiments.

DOI: 10.1103/PhysRevB.88.235121 PACS number(s): 73.21.Cd, 72.15.Qm, 75.20.Hr

I. INTRODUCTION

Dimensionality plays a crucial role in condensed matter physics, especially in systems with strong interactions. In most systems the dimensionality is determined by the structure of the material and cannot be changed. However, in order to study the effects of dimensionality, it would be desirable to control it. Layered structures provide such an opportunity and make it possible to observe effects of reduced dimensionality and crossover behavior between two and three dimensions. In particular, recent successful fabrications of the layered superlattices of $CeIn_3/LaIn_3$[1] and $CeCoIn_5/YbCoIn_5$[2,3] have opened new possibilities for investigating such phenomena in f-electron systems. In these systems, the f electrons are present only in the Ce layers, which are two-dimensional (2D). However, if the f electrons are coupled through the conduction electrons of La or Yb layers, the f electrons effectively become three-dimensional (3D).

This question is also relevant for possible long range order of the f electrons. In the $CeIn_3(n)/LaIn_3(4)$ superlattice,[1] it was reported that, when the Ce layer thickness n is reduced to $n = 2$, the Néel temperature T_N is decreased to zero and the resistivity ρ_{xx} shows linear temperature dependence $\rho_{xx} \sim T$. This non-Fermi-liquid like behavior, which is also found in cuprates with 2D character, is in contrast to the Fermi-liquid like behavior, $\rho_{xx} \sim T^2$, found for large n. This suggests that the Ce layers are coupled and exhibit 3D antiferromagnetism (AF) when n is large, while the coupling between the Ce layers is suppressed for smaller n and the Ce layers retain 2D character.

Furthermore, superconductivity (SC) is reported for the $CeCoIn_5(n)/YbCoIn_5(5)$ superlattice.[2,3] For $CeCoIn_5(n)$-layer thickness $n \geqslant 3$, clear SC transitions are found. In particular, for $n = 5$, the field angle dependence of the upper critical field H_{c2} slightly below the transition temperature can be well fitted by the 3D anisotropic mass model. In contrast, for $n = 3$, the 3D anisotropic mass model can no longer explain H_{c2}, and H_{c2} is well fitted by the Tinkham model for thin superconductors, in which the thickness of the system is smaller than the z-axis SC coherence length.[4] This implies that the superconducting Ce layers are coupled to form a 3D superconductor when n is large, while the coupling is suppressed for smaller n so that the Ce layers remain 2D superconductors.

Magnetism and SC in these layered f-electron superlattices discussed above are interesting problems, many aspects of which are still open. At the same time, these experimental results raise an even more fundamental question of the dimensionality of the heavy electron states due to the f electrons, even in the absence of any order. Theoretical approaches to this problem so far have been based on an implicit assumption that the f electrons, separated by the spacer layers, are almost decoupled, which results in essentially 2D heavy electron states.[5,6] However, whether the heavy electrons in the superlattice are actually 2D or not is a nontrivial issue. Understanding this issue would also be essential in tackling questions about magnetism and SC.

In this paper, we study the formation of the heavy electrons through the Kondo effect and their properties in layered f-electron superlattices. We clarify the dimensionality of the heavy electrons in the superlattice and discuss qualitatively the experimental observations of the AF properties in $CeIn_3/LaIn_3$ and the anomalous H_{c2} in $CeCoIn_5/YbCoIn_5$ based on dimensional crossover.

II. MODEL

In order to capture the essential points of layered f-electron superlattices, we use a model which describes a system with two kinds of layers. One kind of layers includes both c and f electrons (corresponding to Ce layers), and the other kind of layers includes only c electrons (corresponding to La or Yb layers). We call the former type of layers "A layers," and the latter type of spacer layers "B layers." It is noted that the density of states around the Fermi energy in a $CeCoIn_5/YbCoIn_5$ superlattice is almost completely determined by the electrons on the Ce sites and the Yb sites,[2] which validates our model for the superlattices. The numbers of A layers and B layers within the unit cell are given by L_A and L_B, respectively, and $L \equiv L_A + L_B$ is the thickness of the unit cell. Each layer is

represented by a square lattice. The Hamiltonian, which is a variant of the periodic Anderson model (PAM), reads

$$\begin{aligned} H =& -t_c \sum_{izjz'\sigma} c^\dagger_{iz\sigma} c_{jz'\sigma} - t_f \sum_{izjz'\in \mathrm{A},\sigma} f^\dagger_{iz\sigma} f_{jz'\sigma} \\ &+ V \sum_{iz\in\mathrm{A},\sigma} [c^\dagger_{iz\sigma} f_{iz\sigma} + f^\dagger_{iz\sigma} c_{iz\sigma}] \\ &+ U \sum_{iz\in\mathrm{A}} \left[n^f_{iz\uparrow} - 1/2\right]\left[n^f_{iz\downarrow} - 1/2\right], \end{aligned} \tag{1}$$

where $i,j = (x,y)$ correspond to in-plane sites, z is the layer index, and σ is the spin index. Hopping is only allowed between nearest neighbor sites. We set the chemical potentials such that the particle-hole symmetry is conserved. Because $t_f < V < t_c$ is satisfied for the bare parameters in many f-electron systems, we fix them as $t_f = 0.2$, $V = 0.4$ as a typical set of values, taking $t_c = 1$ as the energy unit. We also fix $U = 2.4 = 15V^2/t_c$, which leads to a renormalized hopping $t^*_f = t_f/[1 - \partial\Sigma^{ff}(0)/\partial\omega] \sim 0.03 - 0.04t_c$ in 3D PAM. For these parameters, the resistivities show pronounced peaks when the temperature is changed, as observed in the experiments for bulk $CeIn_3$ and $CeCoIn_5$. The qualitative physics described in this paper is unchanged for different parameters as long as $t_f < V < t_c$ and U is large enough. Note that, due to nonzero t_f, the system is metallic even at half filling. We emphasize that our model is based on a standard model for f-electron systems, PAM, and fully incorporates the superlattice structure. In this respect, the present model is a minimal microscopic Hamiltonian for f-electron superlattices, including both essential ingredients. Because the materials used for different layers in the experimental setup are charge neutral, we do not consider any effects of charge redistribution in this study.

For our Hamiltonian, we have imposed periodic boundary conditions in all directions, so that we can perform Fourier transformation. The Fourier transformation is given by

$$c_{jz\sigma} = \sum_{k_\parallel k_z l} U^c_{j\tilde{z}_1\tilde{z}_2,k_\parallel k_z l} c_{k_\parallel k_z l\sigma}, \tag{2}$$

$$f_{jz\sigma} = \sum_{k_\parallel k_z l} U^f_{j\tilde{z}_1\tilde{z}_2,k_\parallel k_z l} f_{k_\parallel k_z l\sigma}, \tag{3}$$

where the unitary matrices U^c and U^f are defined as

$$U^c_{j\tilde{z}_1\tilde{z}_2,k_\parallel k_z l} = \frac{e^{ik_\parallel R_{j\parallel}}}{\sqrt{N_\parallel}} \frac{e^{ik_z z + iq^c_l \tilde{z}_2}}{\sqrt{N_z}}, \tag{4}$$

$$U^f_{j\tilde{z}_1\tilde{z}_2,k_\parallel k_z l} = \frac{e^{ik_\parallel R_{j\parallel}}}{\sqrt{N_\parallel}} \frac{e^{ik_z z + iq^f_l \tilde{z}_2}}{\sqrt{N_z L_A/L}}. \tag{5}$$

Here $\boldsymbol{k}_\parallel = (k_x,k_y)$ and $\boldsymbol{R}_{j\parallel} = (x_j,y_j)$. The layer index z is parametrized as $z = L\tilde{z}_1 + \tilde{z}_2$ with $0 \leqslant \tilde{z}_2 < L$ for U^c and $0 \leqslant \tilde{z}_2 < L_A$ for U^f. The "orbital" index l is $0 \leqslant l < L(L_A)$ for $U^c(U^f)$, and $q^c_l = 2\pi l/L, q^f_l = 2\pi l/L_A$. The momentum along the z axis is defined in the reduced Brillouin zone (RBZ), $0 \leqslant k_z < 2\pi/L$. $N_\parallel$ is the total number of the sites within a layer and N_z is the total number of the layers. The total number of sites is $N = N_\parallel N_z$. We note that the orbital index l arises from the superlattice structure through the Fourier transformation. Roughly speaking, it specifies where the momentum $K_z = k_z + q^c_l$ is located in the unfolded RBZ $[0,2\pi) = \cup^L_{l=1}[2\pi(l-1)/L, 2\pi l/L)$. We note that only k_z is conserved while K_z is generally not conserved. In the new basis, the Hamiltonian becomes

$$\begin{aligned} H =& \sum_{k\sigma} \sum_{aa',ll'} A^{a\dagger}_{kl\sigma} H^{aa'}_{ll'}(\boldsymbol{k}) A^{a'}_{kl'\sigma} \\ &+ \frac{U}{2NL_A/L} \sum_{\{k_i,l_i\}\sigma} f^\dagger_{k_1 l_1\sigma} f_{k_2 l_2\sigma} f^\dagger_{k_3 l_3\bar{\sigma}} f_{k_4 l_4\bar{\sigma}} \\ &\times \delta_{k_1+k_3,k_2+k_4} \delta_{l_1+l_3,l_2+l_4}, \end{aligned} \tag{6}$$

where $A^{a=c} = c$, $A^{a=f} = f$, and $\boldsymbol{k} = (\boldsymbol{k}_\parallel,k_z)$. The elements of the Hamiltonian are

$$\begin{aligned} H^{cc}_{ll'} =& -2t_c\left[\cos k_x + \cos k_y + \cos\left(k_z + q^c_l\right)\right]\delta_{ll'} \\ & (0 \leqslant l,l' < L), \end{aligned} \tag{7}$$

$$\begin{aligned} H^{ff}_{ll'} =& -2t_f[\cos k_x + \cos k_y]\delta_{ll'} \\ & - t_f S^{ff}_{ll'}\left[e^{-i(k_z+q^f_l)} + e^{i(k_z+q^f_{l'})}\right] \quad (0 \leqslant l,l' < L_A), \end{aligned} \tag{8}$$

$$H^{cf}_{ll'} = V S^{cf}_{ll'} \quad (0 \leqslant l < L, 0 \leqslant l' < L_A), \tag{9}$$

$$H^{fc}_{ll'} = H^{cf*}_{l'l}, \tag{10}$$

where

$$S^{ff}_{ll'} = \frac{1}{L_A} \sum_{z=0}^{z_0} e^{-i(q^f_l - q^f_{l'})z}, \tag{11}$$

$$S^{cf}_{ll'} = \frac{1}{\sqrt{LL_A}} \sum_{z=0}^{L_A-1} e^{-i(q^c_l - q^f_{l'})z}, \tag{12}$$

with $z_0 = L_A - 2$ for $L_B \neq 0$ and $z_0 = L_A - 1$ for $L_B = 0$. We note that none of the elements of $H^{cf,fc}_{ll'}$ vanishes, and therefore all the c electrons are coupled to the f electrons as long as $V \neq 0$. This suggests that all states on the Fermi surface at very low temperature should be composite states of the c electrons and the f electrons.

The Green's functions in this basis are given by

$$G^{aa'}_{ll'}(i\omega_n,\boldsymbol{k}) = -\int_0^{1/T} d\tau \left\langle T_\tau A^a_{kl\sigma}(\tau) A^{a'\dagger}_{kl'\sigma}(0)\right\rangle e^{i\omega_n\tau}. \tag{13}$$

We note that off-diagonal elements $G_{ll'}(l \neq l')$ do not vanish and that these "interorbital" elements include scattering processes between different RBZs. This point is essentially important for understanding the anisotropic behavior in the resistivity, as will be discussed in the next section.

Correlation effects are taken into account by means of the inhomogeneous dynamical mean field theory (DMFT)[7–11] combined with the numerical renormalization group (NRG) as an impurity solver.[12–16] Although the self-energy Σ is site-diagonal, Σ differs for each A layer $\Sigma_{izjz'}(\omega) = \Sigma_z(\omega)\delta_{ij}\delta_{zz'}$ in this approximation. Because DMFT + NRG appropriately takes local correlations into account, the formation of heavy electrons through the Kondo effect is well described by this

method. The self-consistent equation reads

$$\mathcal{G}_z(\omega) = \left[\frac{1}{N_\parallel}\sum_{k_\parallel} G_{zz}(\omega,\boldsymbol{k}_\parallel)\right]^{-1} + \Sigma_z(\omega), \qquad (14)$$

where $\mathcal{G}$ and G are the cavity Green's function and the lattice Green's function, respectively. The lattice Green's function $G_{zz'}(\omega,\boldsymbol{k}_\parallel)$ is obtained by the inverse Fourier transformation with respect to k_z,l from $G_{ll'}(\omega,\boldsymbol{k})$.

III. CALCULATION RESULTS

As was discussed in the previous sections, dimensionality of a superlattice in the paramagnetic normal states is a fundamental property and is a key for understanding the experiments. In this section, we discuss the dimensionality of the system based on our numerical results within the DMFT calculations. In order to clarify the dimensionality, we investigate two measures of dimensionality: band structures of the system and resistivities in different directions.

We start our discussion by analyzing the spectral function

$$A(\omega,\boldsymbol{k}) = -\frac{1}{\pi}\mathrm{tr}[\mathrm{Im}G^R(\omega,\boldsymbol{k})], \qquad (15)$$

where $\boldsymbol{k} = (k_x,k_y,k_z)$ with $0 \leqslant k_{x,y} < 2\pi$ and $0 \leqslant k_z < 2\pi/L$, and G^R is the retarded Green's function. Here, we focus on a $(L_A,L_B) = (2,5)$ superlattice which is exemplary for f-electron superlattices. First, we discuss the shape of the Fermi surface in the superlattice by looking at $A(\omega,\boldsymbol{k})$ for $\omega = 0$. In Fig. 1, we show contour plots of $A(\omega = 0,\boldsymbol{k})$ for $(L_A,L_B) = (2,5)$ at sufficiently low temperature $T = 0.0015$. This temperature is much lower than the coherence temperature so that heavy quasiparticles are well formed in these figures, as will be discussed later. Violet corresponds to high-intensity regions and black corresponds to low-intensity regions. One can compare the Fermi surface in Fig. 1 with the Fermi surface for $V = 0, U = 0$ in Fig. 2 where the c-electron Fermi surface is isotropic and the f electrons have a two-dimensional Fermi surface. Compared to the Fermi surface for $V = 0, U = 0$, the Fermi surface in the superlattice is strongly anisotropic. However, we can clearly see that the Fermi surface in the k_xk_z plane has finite curvatures in Fig. 1. Therefore, we can state that low-energy quasiparticles in the superlattice have finite velocity in the z direction.

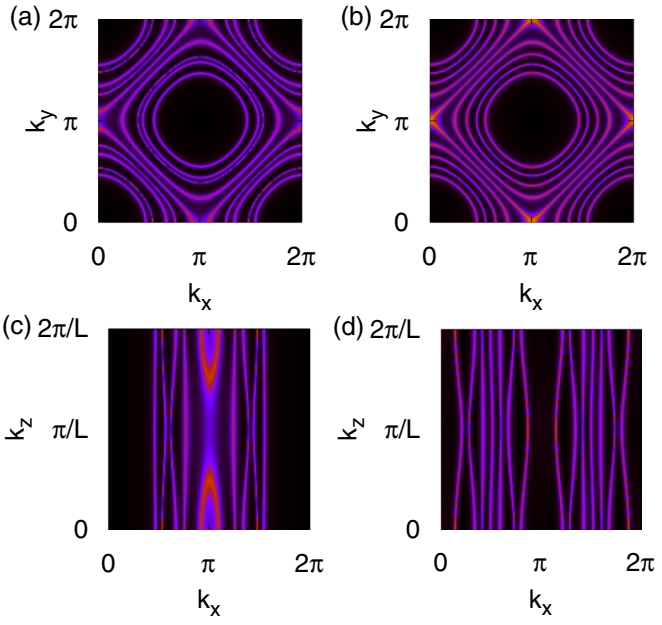

FIG. 1. (Color online) The spectral function $A(\omega = 0,\boldsymbol{k})$ for $(L_A,L_B) = (2,5)$ at (a) $k_z = 0$, (b) $k_z = \pi/2L$, (c) $k_y = 0$, and (d) $k_y = \pi/2$. Temperature is $T = 0.0015$. Violet corresponds to high-intensity regions and black corresponds to low-intensity regions.

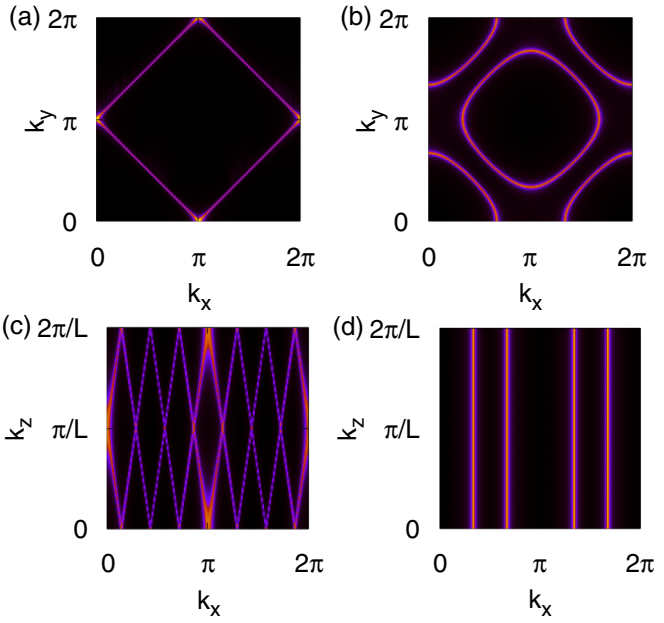

FIG. 2. (Color online) The Fermi surface with $U = 0$, $V = 0$ for (a) c electrons at $K_z = q_1^c + k_z = \pi/2 = 2\pi/7 + 3\pi/14$, (b) f electrons, (c) c electrons at $k_y = \pi/2$, and (d) f electrons at $k_y = \pi/2$. The Fermi surfaces in (a) and (c) are the same. Violet corresponds to high-intensity regions and black corresponds to low-intensity regions.

Indeed, finite curvatures along the z direction are seen in the dispersions of the superlattice. Before discussing the dispersions along the z direction, we show contour plots of $A(\omega,\boldsymbol{k})$ along the x direction for several temperatures at $(k_y,k_z) = (0,\pi/2L)$ for $(L_A,L_B) = (2,5)$ in Fig. 3, as an example. In the present study, a part of a band is called a heavy electron band if its broadening is small enough at low temperatures while it is strongly smeared at high temperatures. At $T = 0.02$, there are no distinguishable heavy electron bands around the Fermi energy $\omega = 0$. On the other hand, for $T = 0.0015$, which is sufficiently lower than the crossover temperature $T_0 \sim 0.01$–0.015, the heavy electron bands are well formed around $\omega = 0$. Note that all the bands especially around $\omega \sim 0$ are altered when the temperature is changed in Fig. 3, which means that the heavy electrons are present in all bands at low temperatures. Next, in Fig. 4, we show the spectral function along the z direction at $(k_x,k_y) = (0.55\pi,0)$ with the same parameters as in Fig. 3. The formation of the heavy electron bands is again observed around $T \sim 0.01$. In order to distinguish the correlation effects in the spectral function, dispersions for the noninteracting case, $U = 0$, are

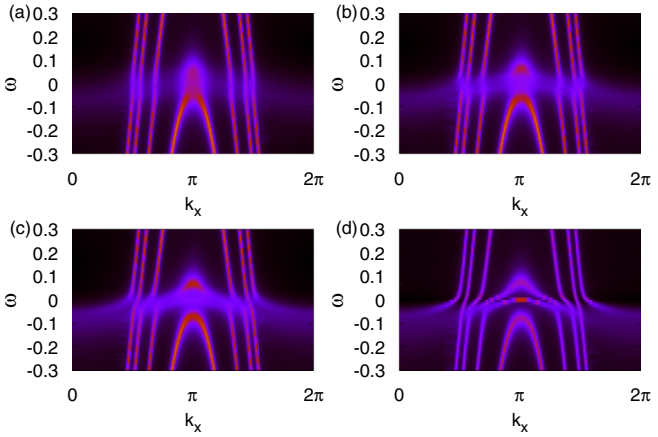

FIG. 3. (Color online) The spectral function $A(\omega,\boldsymbol{k})$ at $(k_y,k_z) = (0,\pi/2L)$ for several temperatures when $(L_A,L_B) = (2,5)$. Temperatures for (a), (b), (c), and (d) are $T = 0.02$, 0.015, 0.01, and 0.0015, respectively. Violet corresponds to high-intensity regions and black corresponds to low-intensity regions.

also shown in Fig. 5 using the same parameters as in Figs. 3 and 4. Interestingly, the correlation effects largely depend on the bands. For example, in Fig. 3(d), the outermost band at $k_x = 0 \sim \pi/2$ is strongly renormalized and broadened compared to other bands. Similarly, in Fig. 4(d), the nearly flat band around $\omega \sim -0.05$ has weaker intensity than those of other bands around $|\omega| \sim 0.05$. In the present superlattice structure, $(L_A,L_B) = (2,5)$, although there is only one kind of the local selfenergy $\Sigma_{z=L\tilde{z}_1} = \Sigma_{z=L\tilde{z}_1+1}$, such band dependence in the spectral function can indeed arise due to the superlattice structure.

As already mentioned above, the heavy electron bands have finite curvature along the z direction. The width of the heavy electron bands along the z direction in Fig. 4 is not negligibly small compared to that along the x direction in Fig. 3. This is the typical behavior for general (k_x,k_y) around the Fermi surface. If the c electrons in the B layers do not participate in the formation of the heavy electrons, heavy bands with

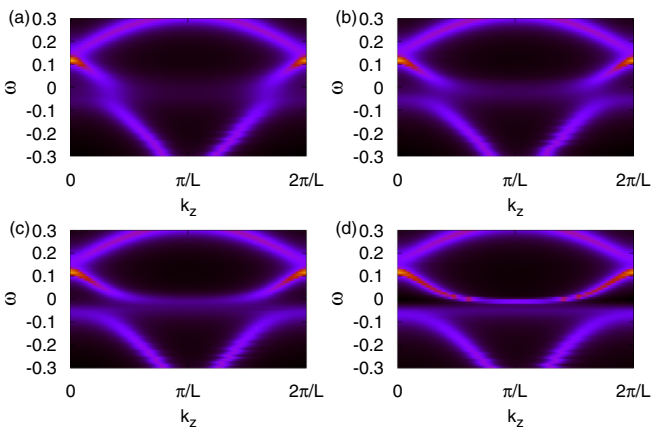

FIG. 4. (Color online) The spectral function $A(\omega,\boldsymbol{k})$ at $(k_x,k_y) = (0.55\pi,0)$ for several temperatures when $(L_A,L_B) = (2,5)$. Temperatures for (a), (b), (c), and (d) are $T = 0.02$, 0.015, 0.01, and 0.0015, respectively.

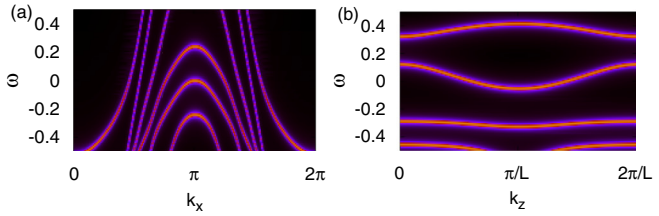

FIG. 5. (Color online) The spectral function $A(\omega,\boldsymbol{k})$ for $U = 0$ (a) at $(k_y,k_z) = (0,\pi/2)$ and (b) at $(k_x,k_y) = (0.55\pi,0)$ for $(L_A,L_B) = (2,5)$.

such a large curvature for the z direction cannot be observed. Indeed, the large curvature in the heavy bands is mainly due to the c-electron hopping which connects separated A layers. Therefore, the heavy electrons are present with significant weight even in the B layers, and the corresponding heavy electron wave functions are extended over the entire system.[17] This is in strong contrast to the implicit assumption in the previous studies[3,6] that the heavy electrons exist only in the Ce layers. We emphasize that the heavy electron bands become observable at the same temperature T_0 both for the x direction and the z direction, which means that there is no distinguishable 2D-3D crossover in the dispersion. In our system, it is expected that any small $V > 0$ makes the f electrons three-dimensional at $T \ll T_0$ (T_0 depends on V), while they cannot coherently move in any direction at $T \gg T_0$. In this sense, looking only at the dispersions, there is no two-dimensional temperature region in our system with $(L_A,L_B) = (2,5)$. For other superlattice structures $(L_A,L_B) = (4,1)$, (3,1), (2,1), (2,2), and (2,3) analyzed in the present study, the dispersions are qualitatively the same as that for $(L_A,L_B) = (2,5)$, although effect of the interaction becomes smaller as a "f-electron layer density" L_A/L is decreased.

However, the formation of the heavy electrons does not directly imply metallic character of the system, which is experimentally defined through transport properties. Theoretically, this is because the former is a one-particle property while the latter is related to two-particle correlations. We thus investigate the resistivity along the x and z directions to clarify the metallic character of the superlattice, which is a direct measure of the dimensionality of the electron motions.

We calculate the resistivity using the Kubo formula. The conductivity in arbitrary units is given by

$$\sigma_{\mu\mu} = \lim_{\omega\to 0}\frac{1}{i\omega}\left[K^R_{\mu\mu}(\omega) - K^R_{\mu\mu}(0)\right], \tag{16}$$

$$K_{\mu\mu}(i\omega_n) = \int_0^{1/T} d\tau \langle T_\tau J_\mu(\tau) J_\mu(0)\rangle e^{i\omega_n\tau}, \tag{17}$$

$$J_\mu = \sum_{k\sigma}\sum_{aa'll'} A^{a\dagger}_{kl\sigma} v^{aa'}_{ll'}(\boldsymbol{k}) A^{a'}_{kl'\sigma}, \tag{18}$$

$$v^{aa'}_{ll',\mu}(\boldsymbol{k}) = \frac{\partial H^{aa'}_{ll'}(\boldsymbol{k})}{\partial k_\mu}. \tag{19}$$

The resistivity is simply calculated by $\rho_{\mu\mu} = 1/\sigma_{\mu\mu}$. In the present study, we neglect the vertex corrections in $K_{\mu\mu}$ because it is known that effects of the vertex corrections on the resistivity are small.[18,19] Under this approximation, $K_{\mu\mu}$ is

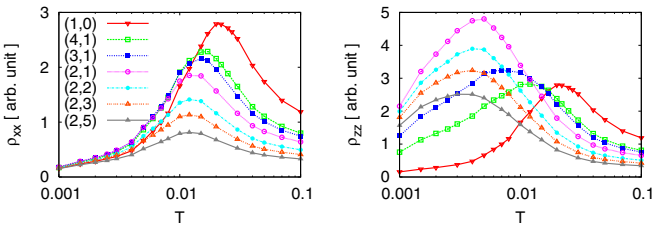

FIG. 6. (Color online) Temperature dependence of the resistivity for the x direction, ρ_{xx} (left panel), and the z direction, ρ_{zz} (right panel). The numbers (L_A,L_B) in the figure denote corresponding layer configurations. For a comparison, the resistivities for the 3D PAM $(L_A,L_B) = (1,0)$ are also shown with red curves.

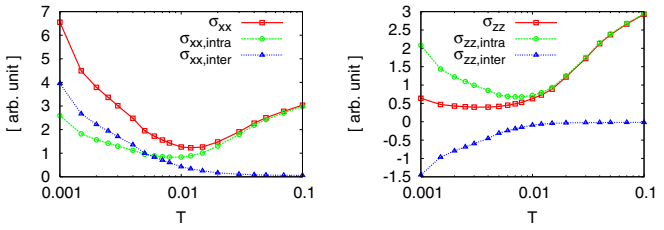

FIG. 7. (Color online) Temperature dependence of the x-axis conductivity (left panel) and z-axis conductivity (right panel) for $(L_A,L_B) = (2,5)$.

evaluated as

$$K_{\mu\mu}(i\omega_n) = -\frac{T}{N}\sum_{aa'=c,f}\sum_{\varepsilon_m \boldsymbol{k},\{l_i\}} v^{aa}_{l_1 l_2 \mu} v^{a'a'}_{l_3 l_4 \mu} G^{a'a}_{l_3 l_2}(i\varepsilon_m,\boldsymbol{k}) \times G^{aa'}_{l_1 l_4}(i\varepsilon_m + i\omega_n,\boldsymbol{k}). \quad (20)$$

After an analytic continuation, we have three terms proportional to $G^R G^R$, $G^A G^A$, and $G^A G^R$, by using the retarded (advanced) Green's functions $G^{R(A)}$.[18] Since it is seen that the $G^{R(A)}G^{R(A)}$ terms are much smaller than the $G^A G^R$ term in the present study, we safely neglect them in the numerical calculations.

In Fig. 6, we show calculation results of the resistivities in the x direction, ρ_{xx}, and in the z direction, ρ_{zz}. For a comparison, the resistivities for the bulk 3D PAM $(L_A,L_B) = (1,0)$ are also shown as red curves. The numbers in the figure (L_A,L_B) represent layer configurations. Similar to the 3D PAM, the resistivities in the superlattice exhibit peak structures at the coherence temperatures below which the electron motions become coherent. For decreasing f-electron layer density L_A/L, the peak height of the in-plane resistivity ρ_{xx} is suppressed and its positions T_x are shifted to lower temperatures compared with those of the bulk 3D PAM, which would be consistent with the experiments.[1,2] In the limit $L_A/L \ll 1$, the conductivity becomes dominated by the c electrons and effects of the interaction between the f electrons get masked. The qualitative agreement with the experiments supports that our model calculations capture the essential physics of f-electron superlattices. If the superlattice is regarded as a junction of a light metal and a heavy metal with largely different Fermi velocities, as in the previous study,[6] the in-plane resistivity is supposed to be determined only by the light metal region resulting in a monotonic temperature dependence,[20] which is in strong contrast to the experiments.[1,2] Qualitatively similar L_A/L dependence of the peak positions T_z is also seen in the z-axis resistivity ρ_{zz}. However, quantitatively, ρ_{zz} much more strongly depends on L_A/L. Furthermore, the coherence temperature for the z axis is lower than that for the x axis in the superlattice, and the difference between both coherence temperatures grows as L_A/L is reduced.

The difference between T_x and T_z can be explained, once the conductivity is divided into "intraorbital" and "interorbital" contributions, $\sigma_{\mu\mu} = \sigma_{\mu\mu,\mathrm{intra}} + \sigma_{\mu\mu,\mathrm{inter}}$. The former is defined by restricting $l_1 = l_2 = l_3 = l_4$ in Eq. (20), and the latter is defined by a sum of all other terms. If we define constituent currents by $j_{\mu,ll'} \equiv \sum_{k\sigma}\sum_{aa'} A^{a\dagger}_{kl\sigma} v^{aa'}_{ll',\mu} A^{a'}_{kl'}$, the separate contributions can be expressed in a simplified notation as $\sigma_{\mathrm{intra}} \sim \sum_l \langle j_{ll} j_{ll}\rangle$ and $\sigma_{\mathrm{inter}} \sim \sum'_{l_1,l_2,l_3,l_4} \langle j_{l_1 l_2} j_{l_3 l_4}\rangle$, where $\sum'_{l_1,l_2,l_3,l_4}$ is defined as a summation over $l_1 \sim l_4$ except for $l_1 = l_2 = l_3 = l_4$. The two contributions describe different transport processes, and each of them alone is not an observable. We note that σ_{intra} must be non-negative, since it is written by a sum of correlation functions of the constituent currents j_{ll} with itself. On the other hand, σ_{inter} does not need to be non-negative, since it is not written only by self-correlations of the constituent currents and it includes other terms like $\langle j_{11} j_{23}\rangle$.

Figure 7 shows $\sigma_{\mu\mu}$, $\sigma_{\mu\mu,\mathrm{intra}}$, and $\sigma_{\mu\mu,\mathrm{inter}}$ for $\mu = x,z$ when $(L_A,L_B) = (2,5)$ as an example. At high temperature $T > T_x$, the conductivities are determined by the intraorbital contributions. We note that $\sigma_{xx,\mathrm{intra}}$ and $\sigma_{zz,\mathrm{intra}}$ exhibit a minimum at the same temperature scale $T_x \simeq T_0$, below which the heavy electrons are well defined. On the other hand, at low temperatures $T < T_x$, the interorbital contributions become important. While $\sigma_{xx,\mathrm{inter}}$ is positive, $\sigma_{zz,\mathrm{inter}}$ is negative at low temperatures, so that it strongly suppresses σ_{zz} for the present parameters. The negative contribution to the total conductivity means that the transport processes corresponding to $\sigma_{zz,\mathrm{inter}}$ increase resistivity. Since $\sigma_{\mu\mu,\mathrm{inter}}$ is mainly determined by $G_{ll'}(l \neq l')$, we conclude that the reduction of the z axis conductivity is due to scattering between different RBZs. Such transport processes give positive contributions to σ_{xx}, because the k_z dependence is not important for the x-direction transport. Namely, the heavy electrons are scattered by the superlattice structures along the z axis resulting in the reduced conductivity σ_{zz}, while such scattering does not affect the in-plane conductivity σ_{xx}.

We now summarize the dependence of the coherence temperatures $T_{x,z}$ on the f-electron layer density L_A/L in Fig. 8. These temperatures correspond to the energy scales for the coherent motion of the heavy electrons in different (x and z) directions. From those, we can draw conclusions about the dimensionality of the heavy electron motions. The L_A/L - T phase diagram has three distinct regions: a high-temperature region ($T > T_x$), a 2D-like region ($T_z < T < T_x$), and an anisotropic 3D-like region ($T < T_z$). In the high-temperature region, the heavy electrons are not well defined. On the other hand, when $T < T_z$, the system is an anisotropic 3D Fermi-liquid metal and the heavy electrons can move coherently in any direction. The most remarkable region, however, is the 2D-like region where coherence is only well developed in the xy plane, while for

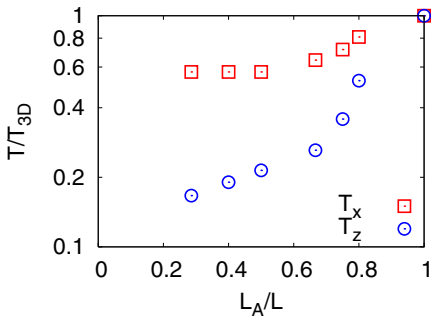

FIG. 8. (Color online) Coherence temperatures vs L_A/L for $(L_A, L_B) = (1,0)$, (4,1), (3,1), (2,1), (2,2), (2,3), and (2,5).

the z direction coherent movement is strongly suppressed. In this region, the heavy electron motions are two-dimensional. As the temperature is lowered for fixed L_A/L, or L_A/L is reduced for fixed temperature, a crossover from two to three dimensions in the behavior of the heavy electrons takes place. In the limit $L_A/L \to 0$ the resistivities are completely dominated by the c electrons and the peaks are smeared, which suggests the system behaves nearly as a 3D free-electron system and there is no longer a clear dimensional crossover.

We emphasize that the dimensional crossover is intrinsic in the superlattice. This can be compared to layered systems without superlattice structures. While σ_{xx} and σ_{zz} differ in magnitude in such systems, their temperature dependence is essentially the same, and T_x, T_z are supposed to coincide.[21] This holds true if the momentum dependence of the self-energy is weak, as in a case of formation of the canonical Fermi liquid.[22] Our results suggest that the superlattice structure is important for observing the dimensional crossover. As far as we know, the present study is the first demonstration of dimensional crossover in f-electron systems. We have revealed the nature of the heavy electrons, which is essential in understanding many physical properties, in layered f-electron superlattices. While most of the present analyses are directly applicable only to the paramagnetic states, they serve as a basis for understanding the intriguing experiments on the ordered states.

IV. DISCUSSION AND SUMMARY

Finally, we give a qualitative discussion on the experiments, based on the dimensional crossover as a possible explanation. For this discussion, we have to keep in mind that T_x and T_z are defined by the resistivities in the normal paramagnetic state, and both of the c, f-electron contributions are important in the transport while f-electron contributions would be crucial in itinerant magnetism and superconductivity. However, the dimensionality in the transport which is a direct measure of the metallic character of the system could be closely related to the z-axis coherence length of the experimentally observed ordered states. When L_A/L is small, magnetic coupling between separated Ce layers is supposed to be suppressed. This leads to low Néel temperatures, which is consistent with the experiments in $CeIn_3/LaIn_3$.[1] In such a case, spin fluctuations can exhibit 2D character in some temperature regions.[23,24] Furthermore, the dimensionality of the heavy electrons would also be relevant for H_{c2} of the superconductivity in $CeCoIn_5/YbCoIn_5$ when the orbital depairing is dominant. For small L_A/L, 2D-like movement of the heavy electrons would result in strong field-angle dependence of H_{c2} around the zero-field transition temperature T_{c0} as found in the experiments.[2,3] We point out that this is in sharp contrast to the previously studied normal-metal-superconductor superlattices such as Ni/Cu and V/Ag[25–29] where the anomalous angle dependence of H_{c2} is seen for sufficiently lower temperatures than T_{c0}. Although the present results and the experiments have common tendencies concerning dimensionality and temperature dependence, the discussions of the experiments presented here are merely qualitative. Itinerant magnetic properties and superconducting properties cannot be described within the DMFT + NRG which is used in the present study. Detailed investigations of these properties are left for future studies.

In summary, we have investigated the f-electron layered superlattice within DMFT + NRG. The heavy electrons are formed in the entire system below T_0 as seen in the spectral function. However, we have identified in the resistivity two distinct energy scales for the coherent motion of the heavy electrons satisfying $T_z < T_x \simeq T_0$. The results of ρ_{xx} are qualitatively consistent with the experiments, which supports our model calculations. We find that the heavy electron motions show a dimensional crossover between two- and three-dimensional character. This dimensional crossover would be responsible for the behaviors of the AF and SC in the $CeIn_3/LaIn_3$ and $CeCoIn_5/YbCoIn_5$ superlattices. Our present results thus build the basis for understanding the f-electron superlattice and the related experiments.

ACKNOWLEDGMENTS

We thank Y. Matsuda, T. Shibauchi, H. Shishido, H. Ikeda, H. Kusunose, K. Ueda, S. Fujimoto, and N. Kawakami for valuable discussions. This work is supported by JSPS/MEXT KAKENHI Grants No. 23840009 (Y.T.) and No. 20102008 (M.O.). R.P. thanks the Japan Society for the Promotion of Science (JSPS) for the support by its FIRST Program.

*tada@issp.u-tokyo.ac.jp

[1] H. Shishido, T. Shibauchi, K. Yasu, T. Kato, H. Kontani, T. Terashima, and Y. Matsuda, Science **327**, 980 (2010).

[2] Y. Mizukami, H. Shishido, T. Shibauchi, M. Shimozawa, S. Yasumoto, D. Watanabe, M. Yamashita, H. Ikeda, T. Terashima, H. Kontani *et al.*, Nat. Phys. **7**, 849 (2012).

[3] S. K. Goh, Y. Mizukami, H. Shishido, D. Watanabe, S. Yasumoto, M. Shimozawa, M. Yamashita, T. Terashima, Y. Yanase, T. Shibauchi *et al.*, Phys. Rev. Lett. **109**, 157006 (2012).

[4] M. Tinkham, *Introduction to Superconductivity*, 2nd ed. (McGraw-Hill, New York, 1996).

[5] D. Maruyama, M. Sigrist, and Y. Yanase, J. Phys. Soc. Jpn. **81**, 034702 (2012).

[6]J. H. She and A. V. Balatsky, Phys. Rev. Lett. **109**, 077002 (2012).
[7]A. Georges, G. Kotliar, W. Krauth, and M. Rozenberg, Rev. Mod. Phys. **68**, 13 (1996).
[8]M. Potthoff and W. Nolting, Phys. Rev. B **59**, 2549 (1999).
[9]S. Okamoto and A. J. Millis, Nature (London) **428**, 630 (2004).
[10]R. W. Helmes, T. A. Costi, and A. Rosch, Phys. Rev. Lett. **101**, 066802 (2008).
[11]H. Zenia, J. K. Freericks, H. R. Krishnamurthy, and T. Pruschke, Phys. Rev. Lett. **103**, 116402 (2009).
[12]K. Wilson, Rev. Mod. Phys. **47**, 773 (1975).
[13]R. Bulla, T. Costi, and T. Pruschke, Rev. Mod. Phys. **80**, 395 (2008).
[14]R. Peters, T. Pruschke, and F. B. Anders, Phys. Rev. B **74**, 245114 (2006).
[15]A. Weichselbaum and J. von Delft, Phys. Rev. Lett. **99**, 076402 (2007).
[16]We use $\Lambda = 2$ and $N_{\text{kept}} = 1200$ kept states in the NRG calculations.
[17]R. Peters, Y. Tada, and N. Kawakami, Phys. Rev. B **88**, 155134 (2013).
[18]H. Kontani, Rep. Prog. Phys. **71**, 026501 (2008).
[19]N. Lin, E. Gull, and A. J. Millis, Phys. Rev. B **80**, 161105(R) (2009).
[20]K. Yamada, M. Nakano, K. Yoshida, K. Hanzawa, and A. Sakurai, Prog. Theor. Phys. **82**, 689 (1989).
[21]T. Valla, P. D. Johnson, Z. Yusof, B. Wells, Q. Li, S. M. Loureiro, R. J. Cava, M. Mikami, Y. Mori, M. Yoshimura *et al*., Nature **417**, 627 (2002).
[22]K. Yamada, *Electron Correlation in Metals* (Cambridge University Press, Cambridge, 2004).
[23]H. Kondo, J. Phys. Soc. Jpn. **71**, 3011 (2002).
[24]M. Garst, L. Fritz, A. Rosch, and M. Vojta, Phys. Rev. B **78**, 235118 (2008).
[25]R. A. Klemm, A. Luther, and M. R. Beasley, Phys. Rev. B **12**, 877 (1975).
[26]S. Takahashi and M. Tachiki, Phys. Rev. B **33**, 4620 (1986).
[27]I. Banerjee, Q. S. Yang, C. M. Falco, and I. K. Schuller, Phys. Rev. B **28**, 5037 (1983).
[28]K. Kanoda, H. Mazaki, T. Yamada, N. Hosoito, and T. Shinjo, Phys. Rev. B **33**, 2052 (1986).
[29]B. Y. Jin and J. B. Ketterson, Adv. Phys. **38**, 189 (1989).